VARIOUS WAYS TO TAKE INTO ACCOUNT DENSITY CHANGE IN SOLID-LIQUID PHASE CHANGE MODELS: FORMULATION AND CONSEQUENCES

Jonathan Dallaire, Louis Gosselin*

Département de génie mécanique, Université Laval, Québec City, Québec, Canada, G1V 0A6

Article accepté pour publication dans : International Journal of Heat and Mass Transfer, Volume 103, Décembre 2016.

Abstract

In this paper, a classification of different methods for accommodating volume variations during solid-liquid phase change is presented. The impact of each method is analyzed with the help of a scale analysis. Neglecting fluid velocity at the interface or allowing fluid to enter/exit the domain may result in either local (at the solid-liquid interface) or global (within the system) mass imbalance. This can lead to significant differences in the transient phase change process itself (e.g., 19% more time and 9% more energy to completely solidify a given mass of water with models for which the total mass of the system is conserved). This paper aims at addressing this issue by deriving two new models of thermo-mechanical coupling between the PCM and its container. The first model is that of a PCM bounded by an elastic wall, whereas the second model assumes that a compressible air gap is adjacent to the PCM, which allows the PCM to expand more easily. Analytical expressions are developed for both models and can be used to predict important quantities at equilibrium, such as the position of the solid-liquid interface and the pressure rise within the system. Finally, the two thermo-mechanical coupling models are implemented numerically with a finite volume moving mesh method. Numerical simulations are performed to show the limits of the two models. It is observed that volume variations during phase change can have significant impacts on the evolution of the process.

* Corresponding author: louis.gosselin@gmc.ulaval.ca; Tel.: +1-418-656-7829; Fax: +1-418-656-5343.

Keywords: solid-liquid phase change; melting; solidification; variable density; mass conservation; thermo-mechanical coupling

Nomenclature

c_p	heat capacity [J kg^{-1} K^{-1}]
E	Young's modulus [N m^{-2}]
f	liquid fraction [-]
$\boldsymbol{g}$	gravitational acceleration vector [m^2 s^{-1}]
h_{sl}	latent heat of fusion [J kg^{-1}]
H	height of the one-dimensional slab [m]
k	thermal conductivity [W m^{-1} K^{-1}]
L	length [m]
m''	total mass of the system per unit area [kg m^{-2}]
$\dot{m}''$	liquid mass flux at the solid-liquid interface [kg m^{-2} s^{-1}]
p	pressure [N m^{-2}]
Q''	latent heat flux [W m^{-2}]
q''	heat flux [W m^{-2}]
Ste	Stefan number [-]
t	time [s]
T	temperature [K]
T_C	cold-side temperature [K]
T_H	hot-side temperature [K]
T_m	solidification (or melting) temperature [K]
v	vertical component of the velocity in the liquid phase [m s^{-1}]
v_l	liquid velocity normal to the solid-liquid interface [m s^{-1}]
x, y, z	Cartesian coordinates [m]

Greek Symbols

α	thermal diffusivity [m^2 s^{-1}]
δ	position of the solid-liquid interface [m]

η effective compressibility of the PCM [m^2 N^{-1}]

κ'' effective spring constant [Pa m^{-1}]

ν Poisson coefficient [-]

ρ density [kg m^{-3}]

τ_{diff} diffusion time scale [s]

τ_m solidification/melting time scale [s]

Subscripts

f final value

g gas property

i initial value

l liquid phase property

s solid phase property

w elastic wall property

1. Introduction

Solidification and melting are complex processes in which the state of a substance changes, and as a result, so do its heat transfer properties. Significant differences in terms of thermal conductivity and specific heat are typically observed between the solid and liquid phases of a substance. Similarly, because molecules organize differently in solids or liquids, the density of a substance also changes with its phase. Phase change materials (PCM) either shrink or expand during phase change which can cause a significant impact in terms of deformations and mechanical constraints in the system, as well as on the heat transfer mechanisms themselves.

When developing an analytical or a numerical model, it can be quite a challenge to fully take into account the change of density in solid-liquid phase change processes. The presence of a net mass flux at the solid-liquid interface changes the overall volume of the PCM domain. Solutions to classical problems, such as the Stefan problem, have been developed by assuming a constant density (see, for example, Chapter 11 in [1]), i.e. without considering density change. In fact, in order to simplify the problem, the majority

of analytical or numerical studies on the modeling of melting or solidification assume that the PCM density is the same for both phases, while some studies neglect the net mass flux at the interface (which results in the destruction or generation of mass within the domain over time), see for example [2].

In experimental setups studying phase change, volume change of the PCM during solidification or melting needs to be accounted for even when it is not the main focus of a given study. For example, in their study on the effect of solid subcooling on natural convection melting of pure gallium in a rectangular enclosure [3], Beckermann and Viskanta accommodated volume change during phase change (gallium contracts by about 3% when melting) by allowing liquid gallium to enter the test cell through a small hole in the top wall of the enclosure. This strategy allowed the enclosure to remain completely filled with gallium throughout the experiments, thus minimizing the impact of volume change on the natural convection flow pattern in the enclosure. Braga and Viskanta later performed experiments on the effect of the density extremum on the solidification of water on a vertical wall of a rectangular cavity [4], where the expansion of water upon solidification was accommodated by leaving a small (~3mm) gap at the top of the cavity to allow water to expand without pushing against the inner walls of the cavity. This strategy was also used in Refs. [5] and [6] in the design of experimental apparatus in order to accommodate the expansion of the PCM during phase change.

Volume changes during phase change are also of significant importance in thermal energy storage applications that use PCMs (e.g. encapsulated PCMs). For example, Lopez et al. [7] developed one-dimensional models (assuming spherical symmetry) to understand salt melting within graphite matrices. The thermo-mechanical models developed by the authors are based on mass and energy conservation equations (enthalpy formulation with variable melting temperature and latent heat of fusion), pressure-dependent liquid-crystal equilibriums, isotropic and linear elasticity laws and Poiseuille-like flows. The model explains some of the main observations for the melting of salts within spherical shells made of graphite (e.g. melting within a wide range of temperatures, incomplete melting and loss of heat storage capacity). The models developed in [7] were then extended by Pitié et al. [8] to represent the confined melting of PCMs coated by silicon carbide. Models from [7] and [8] were specifically developed

to study the thermo-mechanical behavior of encapsulated PCMs in thermal energy storage systems.

In their study on the planar solidification of a finite slab, Conti [9] and Conti et al. [10] developed a thermo-mechanical model which was used to determine the effects of pressure on the solidification process as the PCM expanded while constrained by an elastic wall. However, as will be explained in more details below, some assumptions made while developing their model made it valid only under a restrictive set of conditions. In addition, the authors assumed the PCM to be compressible, but used a constant density for each phase, which resulted in a non-conservation of the total mass of the system.

More recently, an experimental and numerical study on melting in a spherical shell al has been performed by Assis et al. [11]. A constant density was used for each phase, and it was assumed that the density varied linearly between the solid and liquid density within the mushy region. A large air cavity was modeled at the top of the PCM to allow the latter to expand during melting. Since both the PCM and the air are assumed to be incompressible, an additional small opening was modeled at the top of the air cavity to allow it to leave the computational domain as the PCM expands. In order to represent the moving interface between the PCM and the air cavity, a volume-of-fluid model was used. The same approach has been adopted by Shmueli et al. [12] for an experimental and numerical study on melting in a vertical cylinder tube. Even though the numerical results from both works are in good agreement with the experiments performed by the authors, they do not address the thermo-mechanical coupling between the PCM and its boundaries, i.e. there is no pressure rise within the system caused by the expansion of the PCM, which could influence the melting properties.

Similarly, an experimental and numerical study on the melting process of PCMs in a rectangular enclosure was recently performed by Ho et al. [13]. In their work, the expansion of the PCM during melting is addressed by allowing the top boundary to move freely while maintaining the two vertical walls and the bottom wall stationary. The authors present experimental and numerical results for a wide range of subcooling, Stefan, and Rayleigh numbers. The numerical predictions are in good agreement with the experimental results. However, the experiments and numerical simulations performed in

their work do not include thermo-mechanical coupling between the PCM and the cavity boundaries.

Kowalczyk et al. [14] studied solid-liquid phase change at high pressure. Recognizing that melting point and latent heat can be influenced by pressure, they proposed a model with pressure-dependant properties. Nevertheless, density was assumed constant in their model and their experimental set-up had a volume adaptation approach in order to control the pressure level due to expansion of water during phase change.

Bilir and Ilken [15] studied numerically the solidification time of PCM in enclosures. Despite the fact that the PCM is physically bounded by the walls of the container, the density was assumed to be the same for both phases in such a way that no pressure build up due to the PCM expansion was accounted for in the heat transfer process. Similarly, the solid-liquid phase change numerical model developed in Wang et al. [16] also assumes that both phases have the same density.

In their review, Sharma et al. [17] describe the typical numerical model used in literature. Their presentation is based on the assumption of a constant density. Nevertheless, they mention in Section 5.7 that "generally phase change materials […] expand on melting and therefore, the design of a suitable heat exchanger is an important component of a latent heat storage system".

In addition to energy storage units, several other applications and situations involve solid-liquid phase change with density change, which can represent modeling challenges. For example, Aschwanden et al. [18] proposed an enthalpy formulation applicable to glaciology, a domain in which water experiences phase change at different levels of pressure and in which thermomechanical coupling could be important. Nevertheless, their comprehensive model relies on a mixture density that is assumed constant. Pham [19] explains in his review on modeling heat and mass transfer in frozen foods that the freezing point and latent heat both decrease with pressure, which should be taken into account in models. Furthermore, according to Pham, thermomechanical coupling and stress calculation are of great importance in freezing processes, and simulation results can be quite different depending on the assumptions that are made with that respect.

Even though considering the PCM density as constant in a model can be deemed a reasonable assumption in some cases, it also makes it impossible to simulate some

important physical behaviors that may result from the expansion or contraction of the PCM during phase change, such as the thermo-mechanical coupling between the PCM and its container. Whenever different densities for the solid and liquid phases are considered, the choice of a proper mass accommodation method is crucial. In the first part of this paper, a classification of different methods for accommodating volume changes in numerical models is presented, namely: (i) neglecting the mass flux at the solid-liquid interface, (ii) an open boundary, (iii) a free boundary, and (iv) thermo-mechanical coupling. These methods will be described and formulated mathematically in the following sections. A scale analysis is proposed to predict how the phase change process will be affected by each approach. In the last part of this paper, the mass accommodation methods are pushed one step further by introducing two new thermo-mechanical coupling models. In addition, numerical simulations are performed for a one dimensional problem to show the impact of the new thermo-mechanical coupling models, and simple analytical tools are developed to predict important physical quantities when the system reaches equilibrium. It is important to mention that the goal of this paper is not to present a specific system, but rather to introduce the fundamentals of phase change problems with density change including thermo-mechanical coupling. The paper could be seen as a generalization of the Stefan problem to situations involving density change during phase change.

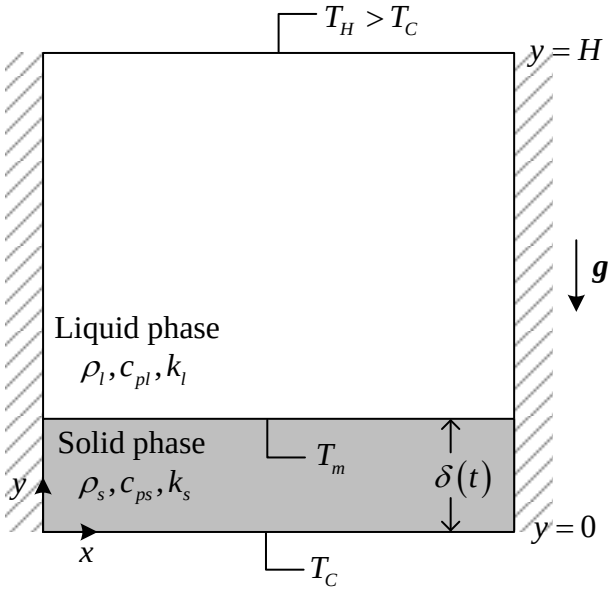

Figure 1

2. Description of the problem

In order to illustrate the classification and models developed in this paper, the following classical problem was addressed: consider a PCM slab of finite thickness H initially liquid and at a temperature $T_i = T_m^+$ slightly higher than the solidification temperature T_m, as depicted in Fig. 1. At time $t = 0$, the temperature of the bottom boundary is suddenly lowered to $T_C < T_m$ while the temperature of the top boundary is maintained at $T_H = T_m^+$. Both left and right boundaries are insulated and thus, the resulting heat transfer problem is one-dimensional. With the current configuration, a thermal stratification occurs in the liquid phase, where cold liquid remains at the bottom, near the solid-liquid interface, and hot liquid remains at the top. Consequently, there will be no natural convection within the liquid phase.

Since all phase change materials have a different density for their solid and liquid phases, they will either expand ($\rho_s < \rho_l$) or shrink ($\rho_s > \rho_l$) as the solidification process goes on, which could cause deformation of the boundaries, leaks, or infiltrations. In order to satisfy mass conservation at the phase change interface during the solidification process with $\rho_s \neq \rho_l$, models should take into account the net mass flux from the solid phase to the liquid phase when $\rho_s < \rho_l$, or inversely, from the liquid phase to the solid phase when $\rho_s > \rho_l$. The expansion or shrinkage of the PCM can also result in a variation of pressure within the domain which will interfere with the phase change process, since both the melting temperature T_m and the latent heat of fusion h_{sl} depend on pressure. In the remainder of this section, the governing equations for the present problem will be briefly stated. In Section 3, commonly used mass accommodation methods will be classified and their respective shortcomings regarding local mass conservation (i.e. at the solid-liquid interface) and global mass conservation (total mass of the system) will be discussed. More advanced mass accommodation methods will be presented at the end of Section 3, where two new thermo-mechanical coupling models will be developed. In addition, simple analytical tools are developed to predict relevant

physical quantities at equilibrium. In Sections 4 and 5, numerical simulations for a one-dimensional problem are performed with those two models, and the numerical results are compared with the analytical predictions from Section 3. Note that even though the analysis performed in this paper is for one dimensional expansion during solidification of PCMs such as water for which $\rho_s < \rho_l$, the reasoning and results can easily be extended to two or three dimensional problems and for other phase change materials with $\rho_s > \rho_l$.

2.1 Governing equations

The energy conservation equations in the solid and liquid phases are given by the two following equations (see Eqs. (11-1a) and (11-1b) in [1]):

$$\rho_s c_{ps} \frac{\partial T_s}{\partial t} = \frac{\partial}{\partial y}\left(k_s \frac{\partial T_s}{\partial y} \right) \tag{1}$$

$$\rho_l c_{pl} \left(\frac{\partial T_l}{\partial t} + v \frac{\partial T_l}{\partial y} \right) = \frac{\partial}{\partial y}\left(k_l \frac{\partial T_l}{\partial y} \right) \tag{2}$$

At the solid-liquid interface, the mass and energy conservation equations when the solid phase density is different from the liquid phase density are expressed as (see Eqs. (11-7a) and (11-8a) in [1]):

$$\rho_l v_l = \left(\rho_l - \rho_s \right) \frac{d\delta}{dt} \tag{3}$$

$$k_s \frac{\partial T_s}{\partial y} - k_l \frac{\partial T_l}{\partial y} = \rho_s h_{sl} \frac{d\delta}{dt} \tag{4}$$

where δ is the position of the solid-liquid interface. In Eq. (3), v_l represents the liquid velocity normal to the solid-liquid interface. Due to the one-dimensional nature of the present problem and to the incompressibility of the PCM, the velocity in the liquid phase will be everywhere the same and equal to v_l for a pure PCM. Note that the solidification or melting rate (right-hand side of Eq. (4)) also takes into account the advection of energy in the liquid phase near the solid-liquid interface even in the absence of forced or natural convection in the melt, since there is a net mass flux at the interface when $\rho_s \neq \rho_l$ (see Section 11-1 in [1]). Finally, the boundary and initial conditions are:

$$T_s\left(y = 0, t \right) = T_C < T_m \tag{5}$$

$$T_s\left(y=\delta,t\right)=T_l\left(y=\delta,t\right)=T_m \tag{6}$$

$$T_l\left(y=H,t\right)=T_H\geq T_m \tag{7}$$

$$T_s\left(0<y<\delta,t=0\right)=T_l\left(\delta<y<H,t=0\right)=T_i \tag{8}$$

2.2 Stefan problem

The Stefan problem is well known and described by the set of equations Eqs. (1)-(2) and (4), provided that ρ is considered equal and constant for both phases. Since there is no density variation during phase change in that case, there is no need to include mass conservation at the solid-liquid interface, i.e. Eq. (3). Exact solutions for the classical Stefan problem can be found in Section 11-2 of [1]. When the time scale for diffusion $\tau_{diff}=H^2/\alpha$ is much smaller than the time scale of the phase change process $\tau_m=\rho h_{sl}H^2/k\left(T_m-T_C\right)$ (i.e. the temperature profile adapts faster than the time required for the slab to solidify or melt), it is known that the position of the solid-liquid interface can be approximated by:

$$\delta\approx\left(2\alpha\ Ste\ t\right)^{1/2} \tag{9}$$

where $\alpha=k/\rho c_p$ is the thermal diffusivity of the PCM and Ste is the Stefan number defined as:

$$Ste\equiv\frac{c_p\left(T_m-T_C\right)}{h_{sl}} \tag{10}$$

The latent heat flux Q'' (the heat flux released during solidification or absorbed during melting) defined as $Q''\equiv\rho_s h_{sl}\,d\delta/dt$ can be expressed using the approximate solution, Eq. (9), which yields:

$$Q''\approx\rho h_{sl}\left(\alpha\ Ste/2t\right)^{1/2} \tag{11}$$

The results obtained from the Stefan problem for the position of the solid-liquid interface and the latent heat flux, i.e. Eqs. (9) and (11), will be compared to the results obtained for other cases in the next sections.

3. Mass accommodation methods

This section presents a classification of the commonly used methods to "accommodate" the mass balance when modeling a phase change process with density variations. The first method addresses the effect of neglecting the induced velocity at the phase change interface (Section 3.1). The second and third methods consider an open boundary through which mass is allowed to leave or enter the domain, and a free boundary that can move during phase change, respectively in Sections 3.2 and 3.3. Those three models, however, disregard any mechanical interaction between the PCM and the boundary. Consequently, both the pressure within the PCM and its melting temperature remain constant during the phase change process. New models that consider the thermo-mechanical coupling between the PCM and its container are thus developed in Sections 3.4 and 3.5. In the former model, the wall of the container is assumed to behave elastically. In the latter, an air gap that can be compressed is present between the PCM and the top wall in order to give more space to the PCM for expansion.

3.1 No induced liquid velocity at the phase change interface

For the first approach considered to accommodate the different phase densities, the induced velocity in the liquid at the phase change interface, represented by Eq. (3), is neglected (this modeling approach is different than the Stefan problem since it considers distinct values of the density in each phase). The result of this simplification is the net creation or destruction of mass at the solid-liquid interface as the phase change process goes on, which means that neither the mass balance at the interface nor the total mass of the system is conserved. Since the induced velocity at the solid-liquid interface is neglected, the resulting velocity in the liquid phase will also be zero everywhere in the system of Fig. 1. This method has been used regularly in the past (e.g., [2]), but the mass conservation issue has not always been addressed explicitly.

For the scale analysis with this approach, the same assumption as in Section 2.2 is used, i.e. the time scale of diffusion $\tau_{diff} = H^2/\alpha_s$ is much smaller than the time scale of the phase change process $\tau_m = \rho_s h_{sl} H^2/k_s(T_m - T_C)$. In other words, the following

analysis is only valid for small Stefan numbers, where $Ste = \tau_{diff} / \tau_m$. Using Eq. (4), it is possible to estimate that the heat flux in the solid phase scales as $q_s'' \sim k_s (T_m - T_C)/\delta$. Assuming that the system is initially at a temperature $T_i = T_m^+$ slightly higher than the solidification temperature and that $T_H \approx T_m^+$, then the heat flux in the liquid phase is $q_l'' \approx 0$ and Eq. (4) becomes:

$$\frac{k_s \left(T_m - T_C\right)}{\delta} \sim \rho_s h_{sl} \frac{\delta}{t} \tag{12}$$

Isolating δ in Eq. (12) gives:

$$\delta \sim \left[\frac{k_s \left(T_m - T_C\right) t}{\rho_s h_{sl}} \right]^{1/2} \tag{13}$$

Using a definition for the Stefan number based on the solid phase properties, i.e. $Ste_s \equiv c_{ps} (T_m - T_C)/h_{sl}$, the last equation can be rewritten as:

$$\delta \sim \left(\alpha_s Ste_s t\right)^{1/2} \tag{14}$$

Similarly to the classical Stefan problem, Eq. (9), the solid-liquid interface position evolves as $\delta \propto t^{1/2}$. The difference with the classical Stefan problem in this case is that the propagation of the phase change interface depends on the solid phase properties only, which comes naturally from the fact that the temperature gradient is only significant in the solid phase throughout the solidification process. Using the definition of the latent heat flux with Eq. (14) for the order of magnitude of δ, one can find that the latent heat flux scales as:

$$Q'' \sim \rho_s h_{sl} \left(\alpha_s Ste_s / t\right)^{1/2} \tag{15}$$

As for the position of the solid-liquid interface, the main difference with the classical Stefan problem comes from the dependence of the latent heat flux on the solid phase properties only. The same behavior, i.e. $Q'' \propto t^{-1/2}$, is observed in the present case.

The initial assumption, however, has the unrealistic consequence that the total mass of the system decreases or increases with time: mass is destroyed or created at the solid-liquid interface due to the different phase densities. It is possible to estimate the rate at

which mass is removed or added to the system per unit area (normal to the solid-liquid interface):

$$\dot{m}'' = \rho_l v_l \tag{16}$$

where v_l in Eq. (16) is the liquid velocity normal to the solid-liquid interface that would actually be present but that is not taken into account in this approach, which gives:

$$\dot{m}'' \sim \left(\rho_l - \rho_s\right)\left(\alpha_s Ste_s / t\right)^{1/2} \tag{17}$$

where $\dot{m}'' > 0$ means that the excess mass that would normally be added to the liquid is now destroyed at the solid-liquid interface, and vice-versa. Thus, the rate of mass destruction or creation at the solid-liquid interface evolves similarly to the latent heat flux, i.e. $\dot{m}'' \propto t^{-1/2}$. Recognizing that the total mass created or destroyed (per unit area perpendicular to the solid-liquid interface) can be obtained by integrating $\dot{m}''$ over time, it follows that the total mass of the system will either increase or decrease proportionally to $t^{1/2}$.

3.2 Open boundary (top surface)

Another approach to accommodate the different phase densities in terms of modeling is to consider the top boundary of the domain as an open surface through which the liquid is allowed to flow in or out, as in Refs. [3]–[6]. This method is rather simple to implement numerically, and as opposed to the previous method, mass is conserved at the solid-liquid interface. However, since mass comes in or out of the system, the total mass of the domain changes. Because of the one-dimensional nature of the problem considered here (Fig. 1), the velocity in the liquid phase will be everywhere equal to the velocity v_l normal to the solid-liquid interface and can be calculated from Eq. (3):

$$v_l = \left(1 - \frac{\rho_s}{\rho_l}\right)\frac{d\delta}{dt} \tag{18}$$

For example, in the case of water with $\rho_s = 918$ kg/m^3 and $\rho_l = 1000$ kg/m^3, the velocity in the liquid is approximately 8% of the velocity of the phase change interface. For the open boundary method, the predictions of the position of the solid-liquid interface δ and the latent heat flux Q'' remain as in the previous case. Moreover, the mass flux leaving or

entering the system is equivalent to the rate at which mass was created or destroyed in the previous approach, Eq. (17), which yields the following order of magnitude for the velocity in the liquid phase when combined with Eq. (16):

$$v_l \sim \left(1-\frac{\rho_s}{\rho_l}\right)\left(\alpha_s Ste_s/t\right)^{1/2} \tag{19}$$

It can be noted at this point that for this method, as well as for the previous method, the total time and energy required to completely solidify or melt the PCM will be different from a case where the total mass of the system is conserved. These differences will be addressed below in Section 3.3.

3.3 Free boundary (top surface)

In the previous approach, mass is conserved at the solid-liquid interface, but the total mass in the domain changes with time, which could be undesired when performing numerical simulations of closed systems. A simple way to fix this issue is to consider the top as a free surface rather than as an open surface, as in Refs. [11]–[13]. This method is more complex to implement numerically since it requires an adaptive mesh or other interface tracking approaches.

Assuming that the system of Fig. 1 is initially liquid and that the initial height of the system is H_i, the total mass of the system per unit area (perpendicular to the solid-liquid interface) is initially equal to $m_i'' = \rho_l H_i$. At a later time t during the phase change process, the total mass of the system per unit area is still the same but is expressed as:

$$m''(t) = \rho_s \delta(t) + \rho_l \left[H(t) - \delta(t)\right] = m_i'' \tag{20}$$

giving the following result for the height of the system as a function of time:

$$H(t) - H_i = \left(1-\frac{\rho_s}{\rho_l}\right)\delta(t) \tag{21}$$

If the solidification process was allowed to continue for a sufficiently long period of time, the solid-liquid interface would eventually reach an equilibrium position somewhere between $y = 0$ and $y = H(t_f)$, where t_f is the final time of the transient solidification process. At equilibrium, the latent heat flux is $Q'' = 0$ and the conduction

heat flux in the solid phase $q_s'' \sim k_s(T_m - T_C)/\delta_{eq}$ is equal to the conduction heat flux in the liquid phase $q_l'' \sim k_l(T_H - T_m)/[H(t_f) - \delta_{eq}]$. Using those orders of magnitude in combination with Eq. (4) , it can then be demonstrated that the position of the solid-liquid interface at equilibrium with a free top surface can be expressed as:

$$\frac{\delta_{eq}}{H_i} \sim \left[\frac{\rho_s}{\rho_l} + \frac{k_l \left(T_H - T_m \right)}{k_s \left(T_m - T_C \right)} \right]^{-1} \tag{22}$$

For the case discussed above where $T_H \to T_m$, the equilibrium position of the solid-liquid interface as given by Eq. (22) tends to $\delta_{eq} \to (\rho_l / \rho_s) H_i$, which is equal to the height of the PCM when it has entirely solidified, i.e. $H(t_f) = (\rho_l / \rho_s) H_i$. This result can be obtained from Eq. (21) by posing $\delta(t_f) = H(t_f)$. This means that in the present case, the solidification process will reach equilibrium when the PCM has entirely solidified. Note that this is also true for the two previous methods (i.e., no induced velocity at the interface and open boundary), in which cases one would find $\delta_{eq}/H_i = 1$ since the height of the PCM domain remains constant throughout solidification.

Although the same scaling is obtained for δ, Q'', and v_l with the free top surface method as compared to the previous methods, the time and energy required to reach equilibrium is not the same, since the mass that was destroyed at the interface or evacuated through the open top boundary in the previous methods now needs to be solidified. The time required to entirely solidify the PCM (t_f) with the first two methods can be obtained by posing $\delta(t_f) = H_i$ in Eq. (12) and then by isolating t_f. For the free top surface method, it can be obtained in the same manner, but this time by recognizing that $\delta(t_f) = \left(\rho_l / \rho_s \right) H_i$. The resulting times are given by Eq. (23) with no induced velocity at the interface and open boundary methods, and by Eq. (24) for the free top boundary method:

$$t_f \sim \frac{\rho_s h_{sl} H_i^2}{k_s \left(T_m - T_C \right)} \equiv \tau_m \text{ (no induced velocity at interface or open boundary)} \tag{23}$$

$$t_f \sim \left(\frac{\rho_l}{\rho_s} \right)^2 \tau_m \text{ (free top boundary)} \tag{24}$$

The amount of latent energy required for a complete solidification of the PCM, Q_f'', is found by multiplying the total mass solidified by the latent heat of fusion. Note that since it is assumed that $Ste_s = 1$, the sensible heat contribution is much smaller than the latent heat contribution. Therefore, the total energy required for a complete solidification should be close to the total amount of latent energy removed from the PCM during its solidification. For the first two methods, the total mass solidified is $\rho_s H_i$, whereas for the free top surface, the total mass solidified is $\rho_l H_i$. The total energy required for complete solidification is given by:

$$Q_f'' \sim \rho_s h_{sl} H_i \text{ (no induced velocity at interface or open boundary)} \quad (25)$$

$$Q_f'' \sim \rho_l h_{sl} H_i \text{ (free top boundary)} \quad (26)$$

These orders of magnitude show the interest of using a method that conserves mass properly when performing transient simulations of closed systems, as it could lead to significant differences for the solidification or melting times, as well as for the energy required for the PCM to completely solidify or melt. Using water as an example (with the densities given in Section 3.2), taking the ratio of Eq. (24) to Eq. (23) indicates that the solidification time would be ~19% longer, whereas taking the ratio of Eq. (26) to Eq. (25) leads to a total energy required ~9% higher when using the free top boundary method, as opposed to other methods for which the total mass of the system changes with time.

3.4 Elastic wall model

Another way to take into account density change during phase change is to consider that the top surface behaves as an elastic wall. Assuming an infinite rigidity for the lateral walls (both in x and z directions), the opposing force applied by the top wall on the PCM during its expansion will result in a rise of pressure within the PCM. In general, pressure can affect both the latent heat and the melting temperature. Taking water as an example, the latent heat of fusion is 333.4 kJ/kg for hexagonal ice (0°C, 101.325kPa [20]) and 352.7 kJ/kg for ice VI (81.6°C, 2150 MPa [21]), which represents a relatively small variation of h_{sl} (~5.8%) over a large range of pressure. In this work, it was thus assumed as a first approximation that the enthalpy of fusion was independent of pressure. However, the effect of pressure on the melting temperature was considered. The thermo-

mechanical coupling between the PCM and its boundary is thus accomplished through the variations of the melting temperature with pressure. The relation between the melting temperature, saturation pressure, and latent heat of fusion is given by the Clapeyron equation (see Section 12-3 in [22]):

$$\frac{dP}{dT_m} = \frac{h_{sl}}{T_m\left(1/\rho_l - 1/\rho_s\right)} \tag{27}$$

Under the assumption of constant ρ_s, ρ_l, and h_{sl}, an expression for the temperature of fusion as a function of pressure can be obtained by integrating Eq. (27), which yields the following expression [9]:

$$T_m\left(p - p_i\right) = T_{mi}\exp\left[-\frac{1-\rho_s/\rho_l}{\rho_s h_{sl}}\left(p - p_i\right)\right] \tag{28}$$

Note that correlations could also be used instead of Eq. (28) to express the melting temperature as a function of pressure, such as the Simon equation given in [23] which is derived from experimental data.

Assuming the top wall to behave elastically (small deformation regime, see Section 3.2 in [24]) and using a spring model to represent the action of the wall on the PCM, the pressure rise in this case is given by the modified Hooke's law:

$$p\left(t\right) - p_i = \kappa_w''\left[H\left(t\right) - H_i\right] \tag{29}$$

where κ_w'' is the effective spring constant of the elastic wall in [Pa/m]. It is noteworthy to mention that the spring constant κ_w'' can be linked to the geometry and the mechanical properties of the top wall. For example, the effective spring constant κ_w'' for a 1D elastic top wall as illustrated in Fig. 2a under the plane strain assumption is given by (See Appendix 1):

$$\kappa_w'' = \frac{E_w\left(1-\nu_w\right)}{\left(1+\nu_w\right)\left(1-2\nu_w\right)L_{wi}} \tag{30}$$

where E_w and ν_w are the wall Young's modulus and Poisson coefficient, respectively.

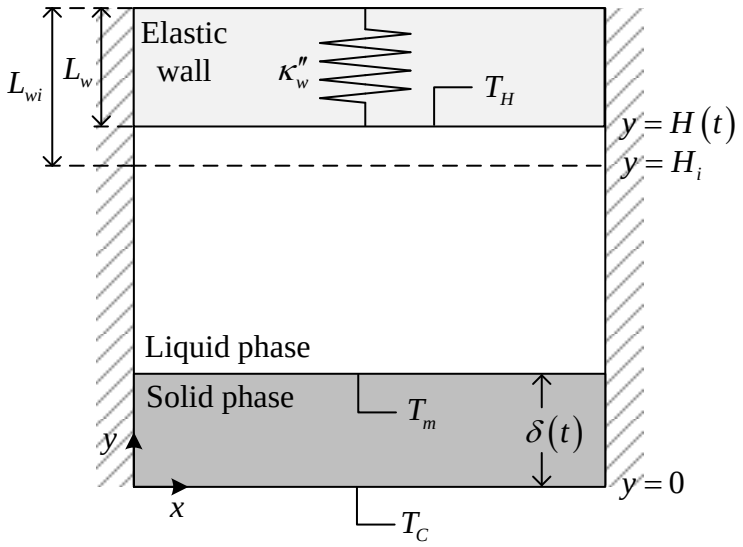

Figure 2a

A similar thermo-mechanical coupling has been attempted by Conti [9] and by Conti et al. [10]. Their model was found to be valid only if the initial length of the wall is the same as the initial length of the PCM and if the Poisson coefficient of the wall is zero, which limits the applicability of their model. The authors further assumed the PCM to be compressible with an effective compressibility for both phases. However, they neglected density variations during compression, resulting in an imbalance of the total mass of the PCM. This can be demonstrated by using the following expression for the total mass of the PCM:

$$m''(t) = \rho_s \delta(t) + \rho_l \left[H(t) - \delta(t) \right] \tag{31}$$

Using the expression for $H(t)$ obtained by combining Eqs. (1) and (4) in [9], Eq. (31) becomes:

$$m'' = m_i'' + (\rho_s - \rho_l) \frac{\eta E_w}{\eta E_w + 1} \delta(t) \tag{32}$$

The second term in Eq. (32) is the mass that will be created if $\rho_s > \rho_l$ or destroyed if $\rho_s < \rho_l$ during solidification. This term will never be zero when $\rho_s \neq \rho_l$ unless $\delta(t) = 0$, in which case there would be no phase change at all.

For these reasons, we found that a novel and more practical model of phase change with thermo-mechanical coupling needed to be developed. In the present model, however, it is assumed that the PCM is incompressible. The first reason for this

assumption is that most PCMs used in practical applications have very small compressibility (e.g. the isothermal compressibility of water is $\eta_{water} \sim 4.6\times10^{-10}\text{Pa}^{-1}$ and that of common ice is $\eta_{ice} \sim 1.1\times10^{-10}\text{Pa}^{-1}$ [25] as opposed to the compressibility of air at atmospheric pressure $\eta_{air} \sim 9.9\times10^{-6}\text{Pa}^{-1}$, see Section 1.7 in [26]). The other reason is that the thermo-mechanical coupling models developed in this paper aim at studying the effect of the density variations during phase change, not density variations due to the compression of the PCMs. As a consequence, the expression given by Eq. (21) can be used to determine the height of the PCM as a function of time, which is required in Eq. (29). The complete mathematical model for the elastic wall consists of the conservation equations (1)-(4), the boundary and initial conditions (5)-(8), and the thermo-mechanical coupling equations, Eqs. (21) and (28)-(30).

In order to assess the importance of an elastic wall at the top boundary and the pressure dependence of the melting temperature, a scale analysis of the equilibrium position of the phase change interface will now be performed. Recognizing that equilibrium is reached when the latent heat flux is zero, i.e. when the heat flux in the solid phase is balanced by the heat flux in the liquid phase, the following expression is obtained:

$$\frac{k_s\left(T_m - T_C\right)}{\delta_{eq}} = \frac{k_l\left(T_H - T_m\right)}{H(t_f) - \delta_{eq}} \tag{33}$$

Then, using a Maclaurin series expansion for the exponential function in Eq. (28), i.e. $\exp(x) \approx 1 + x$ when $x = 1$, yields:

$$T_m\left(p - p_i\right) \approx T_{mi}\left[1 - \frac{1-\rho_s/\rho_l}{\rho_s h_{sl}}\left(p - p_i\right)\right] \tag{34}$$

Combining Eqs. (21), (29) and (34), one finds:

$$T_m\left(p - p_i\right) \approx T_{mi}\left[1 - \frac{\left(1-\rho_s/\rho_l\right)^2 \kappa_w''}{\rho_s h_{sl}}\delta_{eq}\right] \tag{35}$$

which is valid when the following condition is respected:

$$\frac{\left(1-\rho_s/\rho_l\right)^2 \kappa_w''}{\rho_s h_{sl}}\delta_{eq} = 1 \tag{36}$$

Therefore, the approximate solution is valid when the melting temperature of the PCM at equilibrium is not too far from the initial melting temperature. Substituting Eq. (35) into Eq. (33) and using the appropriate expression for $H(t_f)$ based on Eq. (21), the following quadratic equation is obtained:

$$A_w\left(\frac{\delta_{eq}}{H_i}\right)^2 + B_w\left(\frac{\delta_{eq}}{H_i}\right) + C_w = 0 \tag{37}$$

with:

$$A_w = \left(\frac{\rho_s}{\rho_l} - \frac{k_l}{k_s}\right)c_w \tag{38}$$

$$B_w = -\left(\frac{\rho_s}{\rho_l}\frac{a_w}{H_i} + \frac{b_w}{H_i} + c_w\right) \tag{39}$$

$$C_w = \frac{a_w}{H_i} \tag{40}$$

and where:

$$a_w = k_s\left(T_{mi} - T_C\right) \tag{41}$$

$$b_w = k_l\left(T_H - T_{mi}\right) \tag{42}$$

$$c_w = \frac{k_s T_{mi}\left(1-\rho_s/\rho_l\right)^2 \kappa_w''}{\rho_s h_{sl}} \tag{43}$$

It is then possible to solve Eq. (37) to find the equilibrium position of the phase change interface for the elastic wall model. Although solving Eq. (37) is quite easy, the analytical expressions are t. Therefore, these scale analysis results will be presented below, in Section 5, in a graphical form for different values of κ_w'', and compared to a more complete numerical model.

3.5 Air gap model

It is often convenient to leave an air gap (or any other gas) between a PCM and the top wall of its container to accommodate any volume variation induced by a density variation during phase change (see Fig. 2b for the relevant geometrical characteristics of the model). The gas compressibility being much larger than that of the wall or of the

PCM, both boundary deformation and PCM compressibility will be neglected in this model. Therefore, only the compression of air (or any other gas) within the gap is considered. It is also assumed that the pressure is uniform within the system (gas and PCM). The pressure rise within the gas can be obtained from the ideal gas law (Section 3-6 in [22]):

$$\frac{p(t)L_g(t)}{T_g(t)} = \frac{p_i L_{gi}}{T_{gi}} \tag{44}$$

where $T_g(t)$ and T_{gi} are the current and initial average temperature in the gas, whereas $L_g(t)$ and L_{gi} are the current and initial thickness of the air gap, as shown in Fig. 2b. Typically, solidification and melting being slow processes, it is expected that the average temperature of the gas will remain approximately constant during its compression. It is thus assumed in this model that the gas compression by the PCM mainly affects the pressure within the gas, i.e. that Eq. (44) becomes:

$$p(t)L_g(t) = p_i L_{gi} \tag{45}$$

Since the gas will always occupy all the available space between the wall and the PCM, the expression for the thickness of the gas is obtained from:

$$L_{gi} - L_g(t) = H(t) - H_i \tag{46}$$

The pressure rise in the gas (and in the PCM) can be obtained by combining Eqs. (45) and (46), and, after some manipulations, one gets:

$$p(t) - p_i = \kappa_g'' \left[H(t) - H_i \right] \tag{47}$$

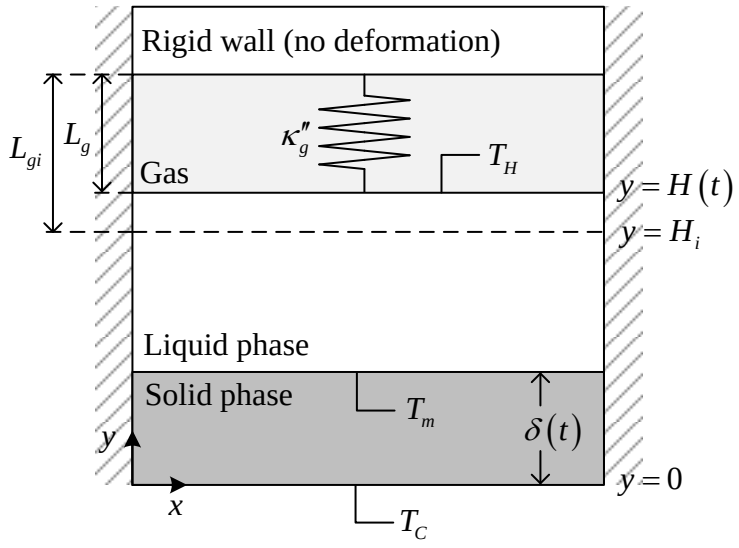

Figure 2b

which is similar to the modified Hooke's law given by Eq. (29) for the elastic wall model, where the gas effective spring constant κ_g'' is given by:

$$\kappa_g'' = \frac{p_i}{L_g(t)} = \frac{p_i}{L_{gi} - (1-\rho_s/\rho_l)\delta(t)} \tag{48}$$

The air gap can thus be seen as a spring with a non-linear effective spring constant that varies as the phase change process goes on. In other words, as the gas within the gap is compressed, it becomes increasingly more difficult to compress it any further. The complete mathematical model for the air gap model consists of the conservation equations (1)-(4), the boundary and initial conditions (5)-(8), and the thermo-gas coupling equations (21), (28), and (47)-(48).

An estimation of the equilibrium position of the solid-liquid interface can be performed for the air gap model by following a similar procedure as for the elastic wall model. However, since the effective spring constant is non-linear (i.e. it is a function of $\delta(t)$), the linearization of Eq. (28) yields:

$$T_m(p - p_i) \approx T_{mi}\left[1 - \frac{(1-\rho_s/\rho_l)^2 p_i \delta_{eq}}{\rho_s h_{sl}\left[L_{gi} - (1-\rho_s/\rho_l)\delta_{eq}\right]}\right] \tag{49}$$

which is valid when the following condition is respected:

$$\frac{(1-\rho_s/\rho_l)^2 p_i \delta_{eq}}{\rho_s h_{sl}\left[L_{gi} - (1-\rho_s/\rho_l)\delta_{eq}\right]} = 1 \tag{50}$$

Once again, the approximate solution for the equilibrium position of the solid-liquid interface is valid when the melting temperature at equilibrium is close to the initial melting temperature. Under these assumptions, the position of the interface at equilibrium is obtained from solving the following quadratic equation:

$$A_g\left(\frac{\delta_{eq}}{H_i}\right)^2 + B_g\left(\frac{\delta_{eq}}{H_i}\right) + C_g = 0 \tag{51}$$

where the coefficients are given by:

$$A_g = k_s\frac{\rho_s}{\rho_l}b_g + k_l d_g \tag{52}$$

$$B_g = -\left[\frac{k_s}{H_i}\left(H_i b_g + \frac{\rho_s}{\rho_l}a_g\right) + \frac{k_l}{H_i}c_g\right] \tag{53}$$

$$C_g = \frac{k_s}{H_i}a_g \tag{54}$$

where:

$$a_g = \left(T_{mi} - T_C\right)L_{gi} \tag{55}$$

$$b_g = \left(1-\rho_s/\rho_l\right)\left[\left(T_{mi} - T_C\right) + \frac{T_{mi}\left(1-\rho_s/\rho_l\right)p_i}{\rho_s h_{sl}}\right] \tag{56}$$

$$c_g = \left(T_H - T_{mi}\right)L_{gi} \tag{57}$$

$$d_g = \left(1-\rho_s/\rho_l\right)\left[\left(T_H - T_{mi}\right) - \frac{T_{mi}\left(1-\rho_s/\rho_l\right)p_i}{\rho_s h_{sl}}\right] \tag{58}$$

Note that the estimation of the equilibrium position of the solid-liquid interface obtained after solving Eq. (51) for the air gap model (or Eq. (37) for the elastic wall model) can be used to estimate other equilibrium quantities. For example, by substituting the estimated value of δ_{eq} in Eq. (21), one can obtain an estimation for the final height of the PCM, i.e. $H(t_f)$, which can then be substituted into Eqs. (29) (elastic wall model) or (47) (air gap model) to get an estimation of the pressure rise within the system at equilibrium. Finally, the estimated pressure rise can be used in Eq. (28) to get an approximation of the melting temperature at equilibrium.

4. Numerical model

In order to illustrate how the mass accommodation techniques and the thermo-mechanical coupling models influence the physical behavior of the system (i.e. pressure rise, variation of the melting temperature, expansion of the PCM, etc.), a series of numerical simulations was performed to complete the scale analysis presented in the previous section. The enthalpy model developed in [27] for solid-liquid phase change with variable density was extended by including the thermo-mechanical coupling methods described in the previous section (i.e., elastic wall and air gap models). In the present numerical model, it was assumed that the phase change process occurred over a narrow temperature range to represent that of a pure PCM. Therefore, there is a small mushy region in which there is mass generation per unit volume. Consequently, even if the problem is one dimensional, there is a velocity gradient within the mushy region and a constant velocity in the pure liquid region. For the sake of concision, the conservation equations for the numerical model will not be repeated here. However, interested readers can find a complete derivation of the equations, as well as explanations on the different assumptions inherent to the numerical model in [27]. Note that even though the equations used for the numerical simulations are expressed in a different form than those used for the analytical predictions in the previous sections, they yield virtually identical results provided that the solidus and liquidus temperatures in the numerical model are both very close to the melting temperature T_m, as demonstrated in Section 7 of [27].

In order to take into account the expansion of the PCM during solidification, a moving mesh method is added to the existing numerical model by moving all the grid points at each time step while keeping the total number of grid points constant. Similar strategies have successfully been used in the past, for example in [28], where a moving mesh method is developed for a two-dimensional heat conduction problem with phase change. Since an enthalpy-porosity method is used, the exact position $\delta(t)$ of the solid-liquid interface is not explicitly calculated. Therefore, instead of using Eq. (21), the height $H(t)$ of the PCM at a given time t is calculated by forcing the conservation of the initial mass of the system and is solved iteratively with the other unknown variables

T, f, v, and T_m. Due to the non-linearity of the problem, under-relaxation is used for both the temperature and the liquid fraction.

The conservation equations are discretized using the finite volume method as described in [29]. Note that the size of each control volume is adapted at each time step to take into account the impact of the moving mesh. On the other hand, a constant time step is used for all simulations. For the advection terms, a central differencing scheme is used since the velocities are expected to be very small, i.e. only a fraction of the solid-liquid interface velocity (which is already small). At each time step, the maximum cell Peclet number is verified and found to be much smaller than 2 for all simulations, which ensures the validity of the chosen differencing scheme. Mesh size and time step were thoroughly tested for all simulations by refining both the mesh size and time step until the impact of any further refinement had a negligible impact on the simulation results. The number of control volumes was set to 300 for all simulations, whereas the time step varied between ~500 s (larger effective spring constants) and ~2000 s (smaller spring constants), depending on the case considered.

Numerical simulations were performed using water as the PCM. The initial height of the PCM slab is $H_i = 0.05\text{m}$ and the following properties are used: $\rho_s = 918\,\text{kg}/\text{m}^3$, $\rho_l = 1000\,\text{kg}/\text{m}^3$, $c_{ps} = 2217\,\text{J}/\text{kg}\cdot\text{K}$, $c_{pl} = 4180\,\text{J}/\text{kg}\cdot\text{K}$, $k_s = 1.92\,\text{W}/\text{m}\cdot\text{K}$, $k_l = 0.58\,\text{W}/\text{m}\cdot\text{K}$, $h_{sl} = 333.4\,\text{kJ}/\text{kg}$. The initial melting temperature of water is $T_{mi} = 273.15\text{K}$ at an initial pressure $p_i = 101.325\text{kPa}$. The solidus and liquidus temperatures in the numerical model are taken as $T_m \pm 0.005\text{K}$. The system is initially liquid at $T_i = 273.155\text{K}$, i.e. at the initial liquidus temperature. At time $t = 0$, the boundary at $x = 0$ is lowered to T_C and is maintained at that temperature for times $t > 0$. The cold-side temperature T_C is calculated with the definition of the Stefan number based on the solid phase properties, i.e. $Ste_s \equiv c_{ps}(T_{mi} - T_C)/h_{sl}$, where the Stefan number for all simulations is $Ste_s = 0.01$. The hot-side temperature is maintained at $T_H = T_i = 273.155\text{K}$ throughout the simulations.

5. Results of numerical simulations

The first case considered is the elastic wall model described in Section 3.4. In order to study the impact of the effective spring constant κ_w'' on the numerical results, the Poisson coefficient ν_w was fixed to 0.35 and the initial length L_{wi} of the 1D elastic wall was fixed to 0.05m for all simulations, while the Young's modulus varied for each simulation. Fig. 3a depicts the position of the solid-liquid interface δ as a function of time for three κ_w'' values, 0.3GPa/m, 3GPa/m, and 30GPa/m. For low values of the effective spring constant κ_w'', the solidification process resembles that of an unconstrained PCM throughout most of the simulation, following the well-known time dependency proportional to $t^{1/2}$. In that case, δ_{eq} tends to $\delta_{eq,free}$, i.e. the equilibrium position of the solid-liquid interface for a free PCM as discussed in Section 3.3 (see Eq. (22)). Note that for very low values of κ_w'', the elastic wall model derived in this papers allows the PCM to solidify beyond its initial height as can be seen in Fig. 3a, which would not be possible if the density of the solid and liquid phases had been the same, or if a model that did not conserve the total mass of the system had been used. When κ_w'' is increased, an asymptotic behavior is found and the equilibrium position of the solid-liquid interface becomes increasingly smaller as the rigidity of the elastic wall augments. For example, a value of $\kappa_w'' = 30\text{GPa/m}$ results in δ_{eq} being smaller than 20% of the initial height of the PCM slab, as shown in Fig 3a. This inhibition of the solidification process comes directly from the fact that as the PCM solidifies and expands, the pressure rise within the system lowers the melting temperature of the PCM until it is too small for the phase change process to continue.

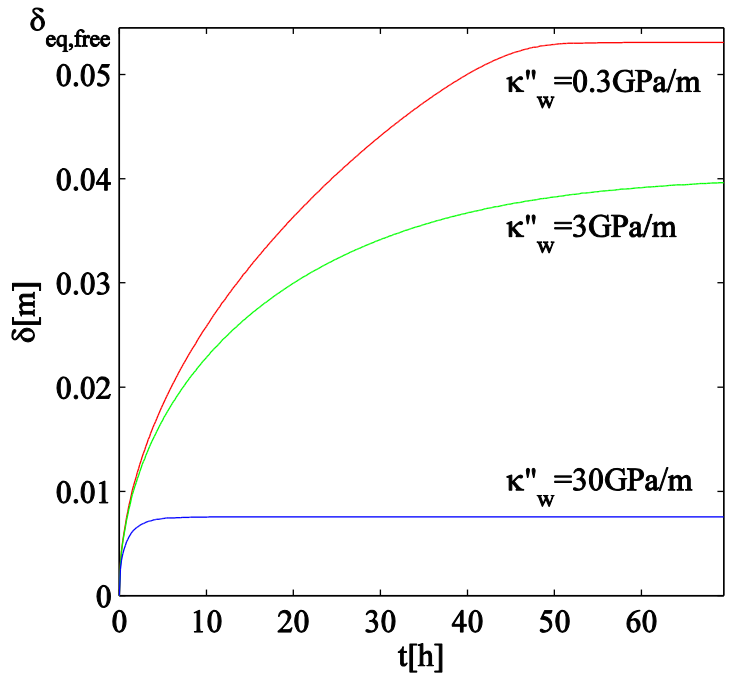

Figure 3a

Figure 3b shows the melting temperature of the PCM as a function of time for the three cases discussed previously. It can be seen that as the effective spring constant increases, the melting temperature of the PCM decreases and gets closer to its physical limit, i.e. the cold-side temperature. In the simulations performed, the changes of the melting temperature were relatively small since the Stefan number of the simulation was small and thus, the cold-side temperature T_C was close to the initial melting temperature. Even though these variations were small, they were enough to hinder the solidification process which resulted in an equilibrium state far from that of an unconstrained PCM. The pressure rise within the system is shown in Fig. 3c for the same values of κ_w''. It can be seen that for moderate to high values of the effective spring constant (3GPa/m and 30GPa/m), the pressure rise can be significant, i.e. 10MPa to 20MPa, which could in certain cases (depending on the material, the geometry, etc.) result in structural breakdown of the container. Note that the pressure rise at equilibrium represents the worst-case scenario, i.e. it is the maximum pressure rise that can occur within the system due to the constrained expansion of the PCM, provided that the integrity of the walls is preserved until the equilibrium state is reached. Therefore, these values could be used as

an estimation of the maximum pressure rise that the system needs to withstand due to the expansion of the PCM during the design process of a container.

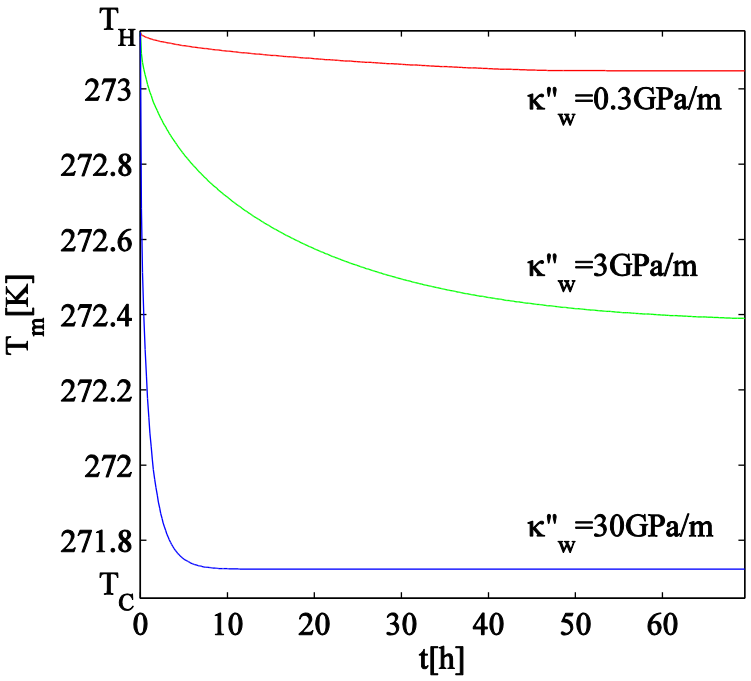

Figure 3b

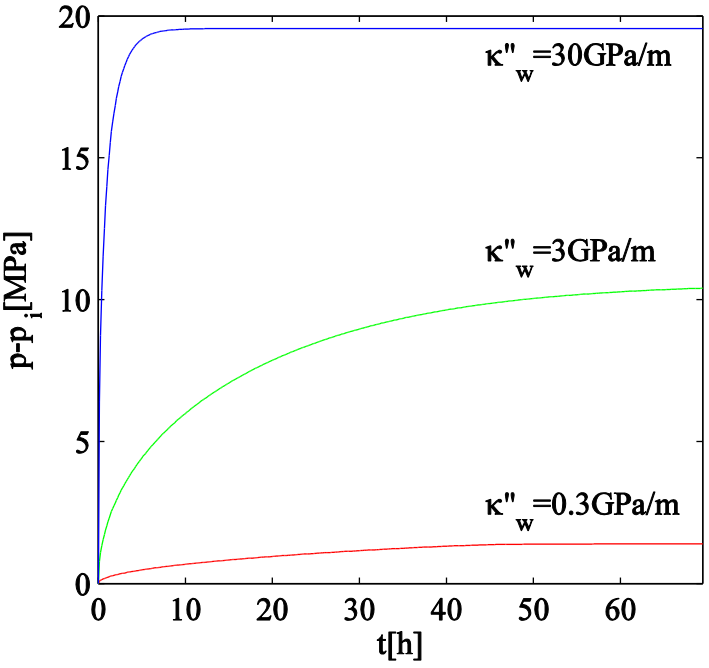

Figure 3c

The second case that was solved with the numerical model is the air gap model derived in Section 3.5. The initial pressure within the gas is the same as that of the PCM, i.e. $p_i = 101.325\text{kPa}$. Since the non-linear effective spring constant of the gas given by Eq. (48) is inversely proportional to the initial length of the gap, L_{gi}, the impact of κ_g'' on the numerical results will be studied by considering different values for L_{gi}. With the physical properties of water used in this paper, the maximum height variation of the PCM at equilibrium (i.e. $H(t_f)-H_i$) is ~4.5 mm and would happen if the PCM was completely free to expand. Therefore, the simulated values of the initial air gap thickness L_{gi} were chosen as 3 mm, 4 mm, and 5 mm, which covered the cases of the gap being too small to allow the PCM to fully expand and cases where the gap was large enough to allow the PCM to expand during solidification.

Figure 4a shows the position of the solid-liquid interface as a function of time for the air gap model and for different values of L_{gi}. As expected, when the air gap is too small to allow the PCM to fully expand (L_{gi} values of 3 mm and 4 mm), the solidification process stops prematurely and δ_{eq} is smaller than the initial height of the PCM. On the other hand, for larger values of L_{gi} and thus, smaller values of κ_g'', the PCM is allowed to solidify almost completely and $\delta_{eq} \to \delta_{eq,free}$, as was the case for small values of κ_w'' for the elastic wall model. However, for the air gap model, the solidification process for all cases follows a very similar path at the beginning of the simulation. As shown in Fig. 4b, the melting temperature of the PCM is relatively similar for all cases considered when the solidification begins. After some time, however, the non-linear behavior of the effective spring used to represent the air gap causes the melting temperature to suddenly drop until the solidification process reaches equilibrium. Similar non-linear behavior is observed for the pressure rise within the PCM, as depicted in Fig. 4c. The pressure rises monotonically at the beginning of the solidification process during which κ_g'' is nearly constant since $\delta(t) = L_{gi}$ in Eq. (48). However, as $\delta(t)$ increases and becomes closer to L_{gi}, then κ_g'' starts increasing rapidly which causes the abrupt pressure rise seen in Fig. 4c. Similarly to the elastic wall model, a significant pressure rise can be observed within the system when

small values of L_{gi} are chosen. However, by selecting an appropriate value of L_{gi} during the design process for a given application, the pressure rise within the system can be controlled. Consequently, it can be large enough to avoid large mechanical constraints that could compromise the structural integrity of the system while being small enough to lower both the size and cost of the system.

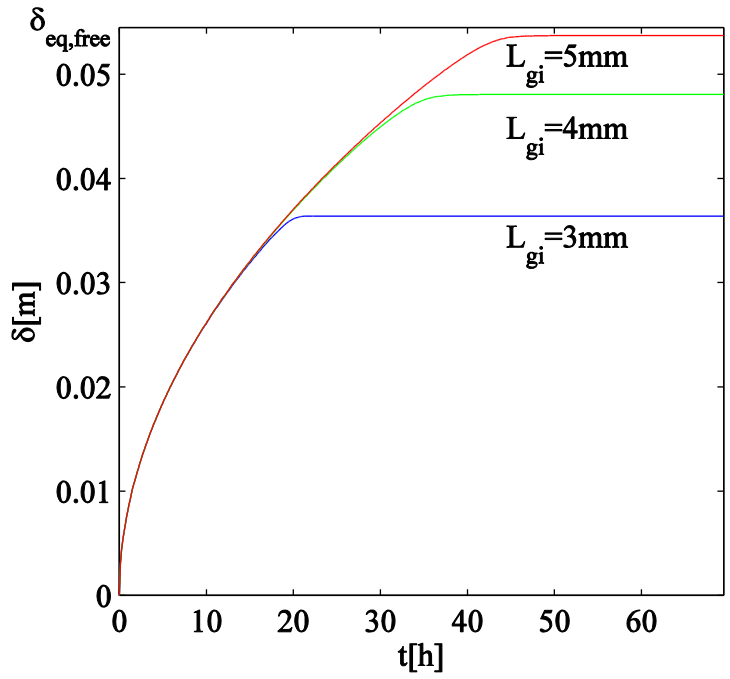

Figure 4a

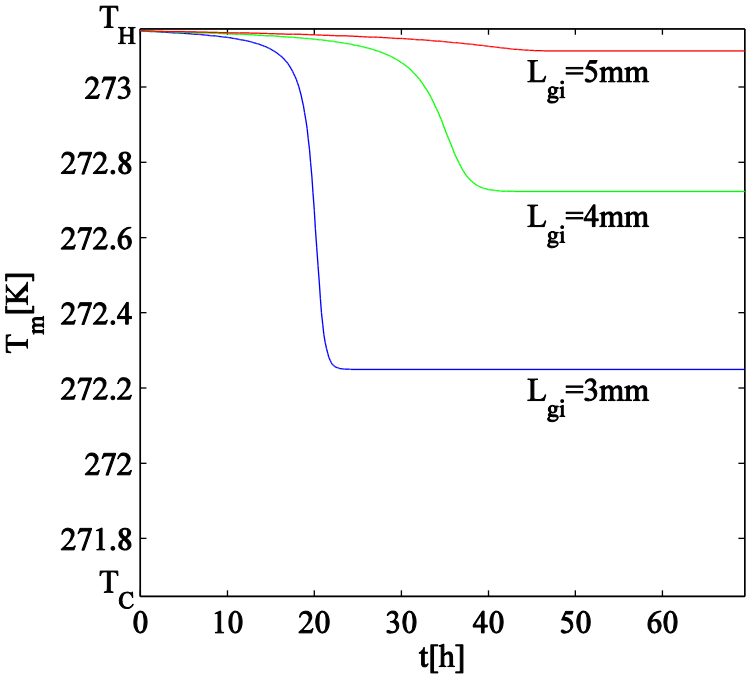

Figure 4b

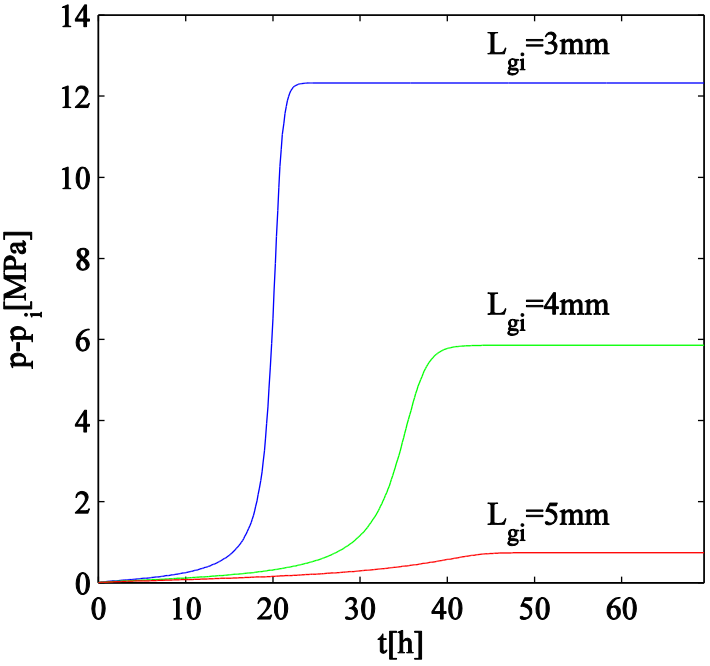

Figure 4c

As was mentioned previously, both the elastic wall and air gap models can be used to predict the important variables related to solidification or melting of a PCM, such as its expansion and the pressure rise within the system. This information is crucial during the design of any given system in order to avoid oversizing and prevent unnecessary costs. The analytical expressions developed in Section 3.4 for the elastic wall model (Eqs. (37)-(43)) and in Section 3.5 for the air gap model (Eqs. (51)-(58)) can be solved easily and can be used to rapidly get such relevant information. The analytical expressions have been compared against numerical simulations for each model. Fig. 5a shows the predicted and simulated equilibrium position of the solid-liquid interface for different values of κ_w'' for the elastic wall model. It can be seen that the scale analysis predictions are in very good agreement with the numerical simulations over a wide range of elastic wall rigidities. Similarly, Fig. 5b shows the predicted and simulated values of δ_{eq} for different initial thickness of the air gap L_{gi}. Once again, the analytical predictions of the equilibrium position of the phase change interface are very close to those obtained through simulation. As mentioned previously, the analytical predictions can also be used to predict other important quantities at equilibrium. For example, predicted values of δ_{eq} have been used in conjunction with Eq. (29) for the elastic wall model and Eq. (47) for the air gap model to predict the pressure rise within the system at equilibrium. Results are shown in Fig. 6a for the elastic wall model and in Fig. 6b for the air gap model. The predicted pressure rises at equilibrium for both models are found to be in very good agreement with the pressure rise obtained from numerical simulations. It is noteworthy to mention that even though they are not presented in this paper, other relevant quantities could be predicted with the analytical expressions developed in Sections 3.4 and 3.5, such as the final height of the PCM slab or the melting temperature at equilibrium.

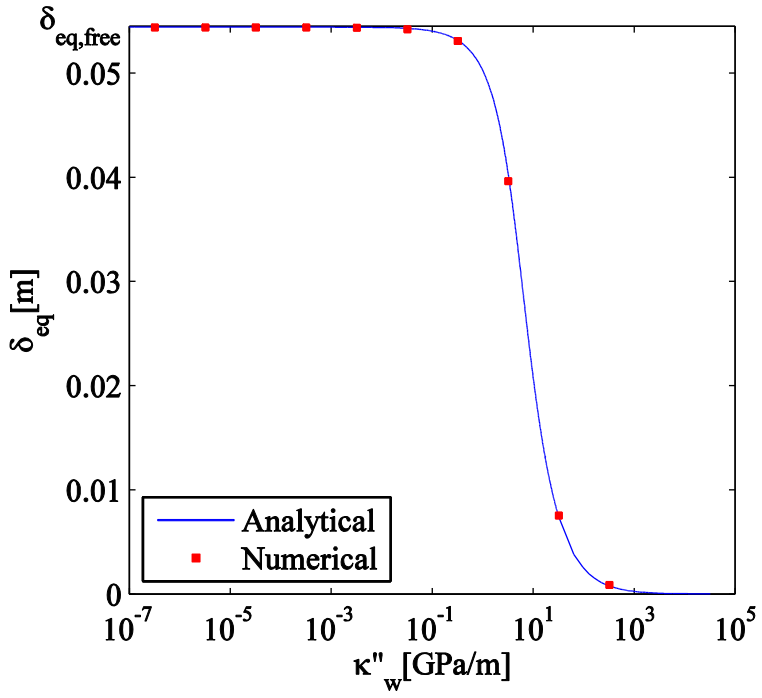

Figure 5a

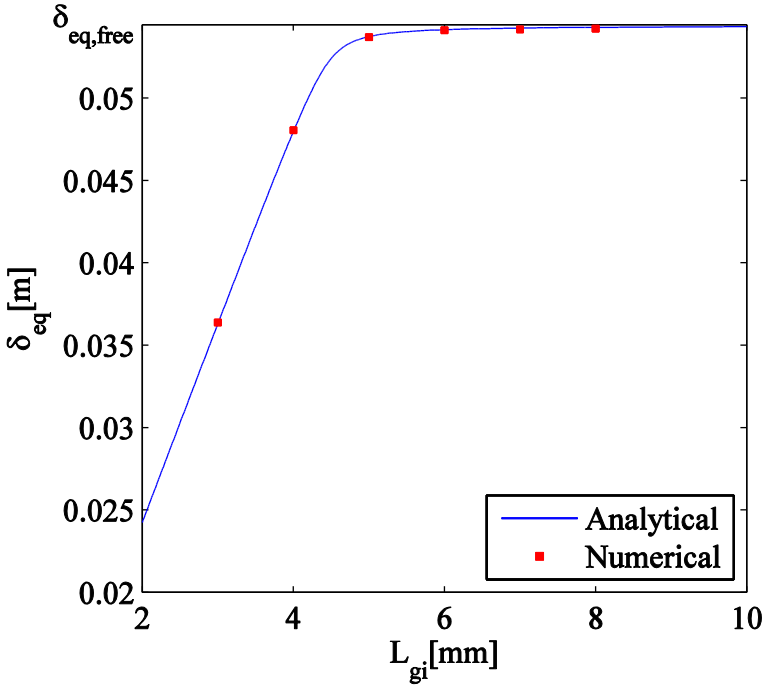

Figure 5b

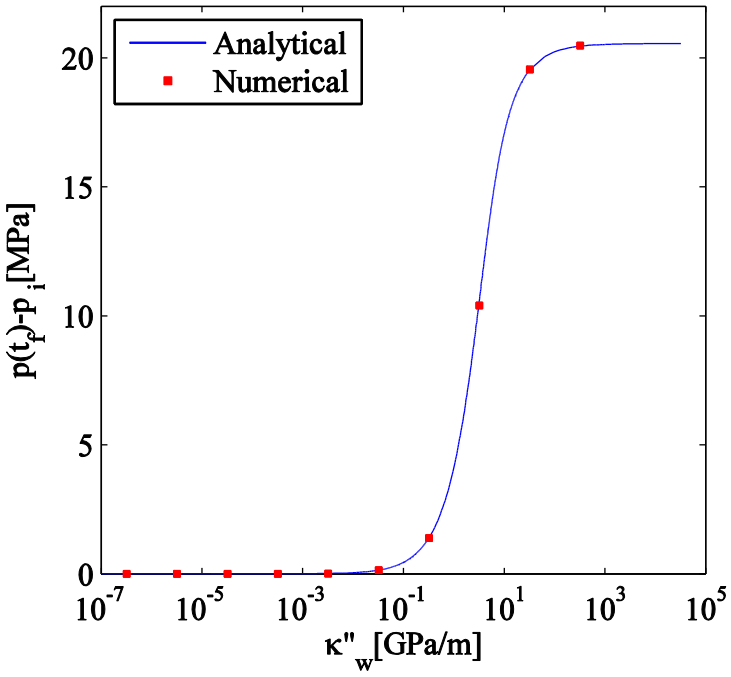

Figure 6a

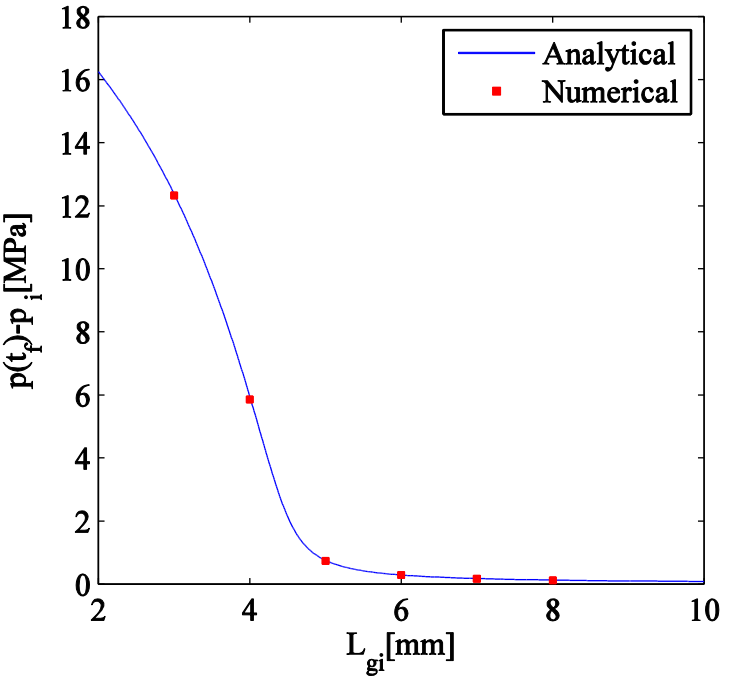

Figure 6b

6. Conclusions

In this paper, various ways of accommodating density variations during solid-liquid phase change were classified and addressed both analytically and numerically for a one dimensional case. It was shown that some assumptions usually found in literature when simulating solid-liquid phase change could lead to imbalance of mass at the solid-liquid interface or within the system. A scale analysis was performed for simple models (no induced velocity at the solid-liquid interface, open top boundary and free top boundary) to predict the behavior of the system in each case. It was also shown that neglecting density variations during phase change could lead to significant differences in the numerical results (e.g. solidification time could be ~19% longer and energy required ~9% higher for the complete solidification of water when density variations were considered).

New models that considered the thermo-mechanical coupling between the PCM and its container were derived. For the first model, it was assumed that the PCM was constrained by a wall that behaved elastically, whereas in the second model, a compressible air gap was introduced to accommodate volume variations during phase change. These two models were implemented numerically with a finite volume moving mesh method and the impact of the models on the transient phase change process were explored by varying the effective spring constant in each case. For both models, the "normal" phase change behavior, i.e. $\delta(t) \propto t^{1/2}$, was replaced by an asymptotic behavior that strongly depended on the value of the effective spring constant of each model. Very low values of κ_w'' and κ_g'' resulted in the PCM behaving similarly to an unconstrained PCM with the equilibrium values similar to the free top boundary model discussed in Section 3.3. On the opposite, large values of these parameters resulted in the solidification process being abruptly interrupted as the pressure rise within the system causes the melting temperature to drop to a point where the system reached equilibrium before the solidification of the entire PCM was completed. Finally, analytical expressions were developed for both models to predict the equilibrium position of the solid-liquid interface and other relevant quantities at equilibrium, such as the melting temperature, the pressure rise or the final height of the PCM.

Acknowledgement

The authors' work is supported by the Natural Sciences and Engineering Research Council of Canada (NSERC).

References

[1] M. N. Ozisik, *Heat Conduction*, 2nd Edition. Wiley-Interscience, 1993.

[2] M. Vynnycky and S. Kimura, “An analytical and numerical study of coupled transient natural convection and solidification in a rectangular enclosure,” *Int. J. Heat Mass Transf.*, vol. 50, no. 25–26, pp. 5204–5214, Dec. 2007.

[3] C. Beckermann and R. Viskanta, “Effect of Solid Subcooling on Natural Convection Melting of a Pure Metal,” *J. Heat Transf.*, vol. 111, no. 2, p. 416, 1989.

[4] S. L. Braga and R. Viskanta, “Effect of density extremum on the solidification of water on a vertical wall of a rectangular cavity,” *Exp. Therm. Fluid Sci.*, vol. 5, no. 6, pp. 703–713, Nov. 1992.

[5] Z. Zongqin and A. Bejan, “Melting in an enclosure heated at constant rate,” *Int. J. Heat Mass Transf.*, vol. 32, no. 6, pp. 1063–1076, Jun. 1989.

[6] Z. Zhang and A. Bejan, “Solidification in the presence of high Rayleigh number convection in an enclosure cooled from the side,” *Int. J. Heat Mass Transf.*, vol. 33, no. 4, pp. 661–671, Apr. 1990.

[7] J. Lopez, G. Caceres, E. Palomo Del Barrio, and W. Jomaa, “Confined melting in deformable porous media: A first attempt to explain the graphite/salt composites behaviour,” *Int. J. Heat Mass Transf.*, vol. 53, no. 5–6, pp. 1195–1207, Feb. 2010.

[8] F. Pitié, C. Y. Zhao, and G. Cáceres, “Thermo-mechanical analysis of ceramic encapsulated phase-change-material (PCM) particles,” *Energy Environ. Sci.*, vol. 4, no. 6, p. 2117, 2011.

[9] M. Conti, “Planar solidification of a finite slab: effects of the pressure dependence of the freezing point,” *Int. J. Heat Mass Transf.*, vol. 38, no. 1, pp. 65–70, Jan. 1995.

[10] M. Conti, F. Marinozzi, and L. Papagno, “Pressure effects in the planar solidification of a finite slab: convective cooling and prescribed heat flux boundary conditions,” *Il Nuovo Cimento C*, vol. 19, no. 2, pp. 257–270, Mar. 1996.

[11] E. Assis, L. Katsman, G. Ziskind, and R. Letan, “Numerical and experimental study of melting in a spherical shell,” *Int. J. Heat Mass Transf.*, vol. 50, no. 9–10, pp. 1790–1804, May 2007.

[12] H. Shmueli, G. Ziskind, and R. Letan, “Melting in a vertical cylindrical tube: Numerical investigation and comparison with experiments,” *Int. J. Heat Mass Transf.*, vol. 53, no. 19–20, pp. 4082–4091, Sep. 2010.

[13] C. J. Ho, K. C. Liu, and W.-M. Yan, “Melting processes of phase change materials in an enclosure with a free-moving ceiling: An experimental and numerical study,” *Int. J. Heat Mass Transf.*, vol. 86, pp. 780–786, Jul. 2015.

[14] W. Kowalczyk, C. Hartmann, and A. Delgado, “Modelling and numerical simulation of convection driven high pressure induced phase changes,” *Int. J. Heat Mass Transf.*, vol. 47, no. 5, pp. 1079–1089, Feb. 2004.

[15] L. Bilir and Z. İlken, “Total solidification time of a liquid phase change material enclosed in cylindrical/spherical containers,” *Appl. Therm. Eng.*, vol. 25, no. 10, pp. 1488–1502, Jul. 2005.

[16] S. Wang, A. Faghri, and T. L. Bergman, “A comprehensive numerical model for melting with natural convection,” *Int. J. Heat Mass Transf.*, vol. 53, no. 9–10, pp. 1986–2000, Apr. 2010.

[17] A. Sharma, V. V. Tyagi, C. R. Chen, and D. Buddhi, “Review on thermal energy storage with phase change materials and applications,” *Renew. Sustain. Energy Rev.*, vol. 13, no. 2, pp. 318–345, Feb. 2009.

[18] A. Aschwanden, E. Bueler, C. Khroulev, and H. Blatter, “An enthalpy formulation for glaciers and ice sheets,” *J. Glaciol.*, vol. 58, no. 209, pp. 441–457, Jun. 2012.

[19] Q. T. Pham, “Modelling heat and mass transfer in frozen foods: a review,” *Int. J. Refrig.*, vol. 29, no. 6, pp. 876–888, Sep. 2006.
[20] R. Feistel and W. Wagner, “A New Equation of State for H2O Ice Ih,” *J. Phys. Chem. Ref. Data*, vol. 35, no. 2, p. 1021, 2006.
[21] A. D. Molina-García, L. Otero, M. N. Martino, N. E. Zaritzky, J. Arabas, J. Szczepek, and P. D. Sanz, “Ice VI freezing of meat: supercooling and ultrastructural studies,” *Meat Sci.*, vol. 66, no. 3, pp. 709–718, Mar. 2004.
[22] Y. A. Cengel and M. A. Boles, *Thermodynamics: An Engineering Approach*, 7th ed. New-York: McGraw-Hill, 2011.
[23] M. Choukroun and O. Grasset, “Thermodynamic model for water and high-pressure ices up to 2.2 GPa and down to the metastable domain,” *J. Chem. Phys.*, vol. 127, no. 12, p. 124506, 2007.
[24] R. C. Hibbeler, *Mechanics of Materials*, 9th ed. Boston: Prentice Hall, 2013.
[25] V. F. Petrenko and R. W. Whitworth, *Physics of Ice*. Clarendon Press, 1999.
[26] B. R. Munson, D. F. Young, and T. H. Okiishi, *Fundamentals of Fluid Mechanics*, 5th ed. John Wiley & Sons, Inc., 2006.
[27] J. Dallaire and L. Gosselin, “Solid-Liquid Phase Change with Variable Density: Formulation of Conservation Equations with Enthalpy Methods,” *Int. J. Therm. Sci.*, Under review.
[28] G. Beckett, J. A. Mackenzie, and M. L. Robertson, “A Moving Mesh Finite Element Method for the Solution of Two-Dimensional Stefan Problems,” *J. Comput. Phys.*, vol. 168, no. 2, pp. 500–518, Apr. 2001.
[29] S. Patankar, *Numerical Heat Transfer and Fluid Flow*. CRC Press, 1980.
[30] E. Volterra and J. H. Gaines, *Advanced Strength of Materials*. Prentice Hall, 1971.

Figure captions

Figure 1 Schematic representation of the solidification process in a slab of finite thickness

Figure 2 Schematic representations of the advanced methods for accommodating density variations during solid-liquid phase change; a) Elastic wall model and b) Air gap model

Figure 3 Simulation results for the elastic wall model with $Ste_s = 0.01$ and for different values of κ_w''; a) Position of the solid-liquid interface, b) Melting temperature, and c) Pressure rise within the system

Figure 4 Simulation results for the air gap model with $Ste_s = 0.01$ and for different values of L_{gi}; a) Position of the solid-liquid interface, b) Melting temperature, and c) Pressure rise within the system

Figure 5 Comparison between predicted and simulated equilibrium positions of the solid-liquid interface; a) Elastic wall model and b) Air gap model

Figure 6 Comparison between predicted and simulated equilibrium pressure rise within the system; a) Elastic wall model and b) Air gap model

Appendix 1: Spring constant κ_w'' for a 1D elastic wall boundary condition

Hooke's law for a wall made of an isotropic material with Young's modulus E_w and Poisson coefficient ν_w is given by (see Section 1.3 in [30]):

$$\begin{bmatrix} \sigma_{xx} \\ \sigma_{yy} \\ \sigma_{zz} \end{bmatrix} = \frac{E_w}{(1+\nu_w)(1-2\nu_w)} \begin{bmatrix} (1-\nu_w) & \nu_w & \nu_w \\ \nu_w & (1-\nu_w) & \nu_w \\ \nu_w & \nu_w & (1-\nu_w) \end{bmatrix} \begin{bmatrix} \varepsilon_{xx} \\ \varepsilon_{yy} \\ \varepsilon_{zz} \end{bmatrix} \tag{59}$$

If infinite rigidity is assumed in the x and z directions (plane strain approximation), then $\varepsilon_{xx} = \varepsilon_{zz} = 0$ and the expression for the stress in the y direction is given by:

$$\sigma_{yy} = \frac{E_w (1-\nu_w)}{(1+\nu_w)(1-2\nu_w)} \varepsilon_{yy} \tag{60}$$

$$(p - p_i) = \frac{E_w (1-\nu_w)}{(1+\nu_w)(1-2\nu_w)} \left(\frac{L_{wi} - L_w}{L_{wi}} \right) \tag{61}$$

When the elastic wall is modeled as a spring with effective spring constant κ_w'', Hooke's law is written as follow:

$$(p - p_i) = \kappa_w'' (L_{wi} - L_w) \tag{62}$$

By comparing Eqs. (61) and (62), the spring constant for a 1D elastic wall as depicted in Fig. 2 a) is expressed as:

$$\kappa_w'' = \frac{E_w (1-\nu_w)}{(1+\nu_w)(1-2\nu_w) L_{wi}} \tag{63}$$